Acta Cryst A FOUNDATIONS ADVANCES

ISSN 2053-2733

Structure factor for an icosahedral quasicrystal within a statistical approach

Radoslaw Strzalka,* Ireneusz Buganski and Janusz Wolny

Faculty of Physics and Applied Computer Science, AGH University of Science and Technology, al. Mickiewicza 30, Krakow, 30-059, Poland. *Correspondence e-mail: strzalka@fis.agh.edu.pl

Received 4 December 2014
Accepted 22 January 2015

Edited by V. Petříček, Academy of Sciences, Czech Republic

Keywords: icosahedral quasicrystal; primitive icosahedral tiling; average unit cell concept; statistical approach; higher-dimensional analysis; diffraction pattern.

This paper describes a detailed derivation of a structural model for an icosahedral quasicrystal based on a primitive icosahedral tiling (three-dimensional Penrose tiling) within a statistical approach. The average unit cell concept, where all calculations are performed in three-dimensional physical space, is used as an alternative to higher-dimensional analysis. Comprehensive analytical derivation of the structure factor for a primitive icosahedral lattice with monoatomic decoration (atoms placed in the nodes of the lattice only) presents in detail the idea of the statistical approach to icosahedral quasicrystal structure modelling and confirms its full agreement with the higher-dimensional description. The arbitrary decoration scheme is also discussed. The complete structure-factor formula for arbitrarily decorated icosahedral tiling is derived and its correctness is proved. This paper shows in detail the concept of a statistical approach applied to the problem of icosahedral quasicrystal modelling.

1. Introduction

Primitive icosahedral tiling [PIT, also known as Amman–Kramer–Neri tiling (Kramer & Neri, 1984), or simply Ammann tiling (Steurer & Deloudi, 2009)] allows an aperiodic space coverage with icosahedral symmetry (Levine & Steinhardt, 1986; Steinhardt & Ostlund, 1987; Baake & Grimm, 2013). It can be used as a model set for three-dimensional aperiodic icosahedral quasicrystals (i-QCs) with Laue class $m\bar{3}5$ (a Platonian icosahedron is shown in Fig. 1*a*). As an aperiodic tiling, PIT gives a sharp diffraction pattern, which is characteristic of all crystalline and quasicrystalline phases [for the mathematical theory of diffraction of aperiodic structures see Baake & Grimm (2013)]. Icosahedral quasicrystals, first obtained by Shechtman *et al.* (1984), are most common among all quasicrystalline phases (Steurer & Deloudi, 2009). As a simple analogue to thick and thin rhombuses in rhombic Penrose tiling, PIT consists of two golden rhombohedra as structural units – acute and obtuse, denoted as AR and OR, respectively (Levine & Steinhardt, 1984, 1986). They are built from golden rhombuses as facets and their volume ratio is $\tau \sim 1.618$ (the golden mean). In that sense PIT may be considered as a three-dimensional generalization of the rhombic Penrose tiling used for modelling two-dimensional decagonal quasicrystals and called three-dimensional Penrose tiling (Yamamoto, 1996; Steurer & Deloudi, 2009).

The structural modelling of quasicrystals can be described within the higher-dimensional approach. Its main idea is that the low-dimensional aperiodicity vanishes after lifting the structure up to high dimensions (de Bruijn, 1981; de Wolff *et al.*, 1981). The real structure is obtained by a projection of the higher-dimensional periodic set of points onto the lower-

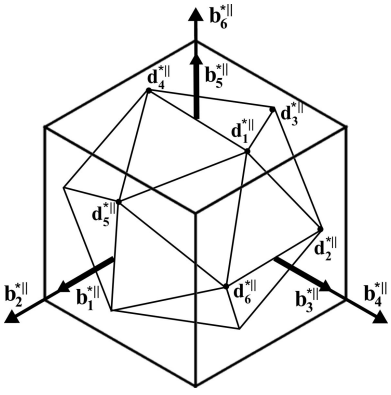

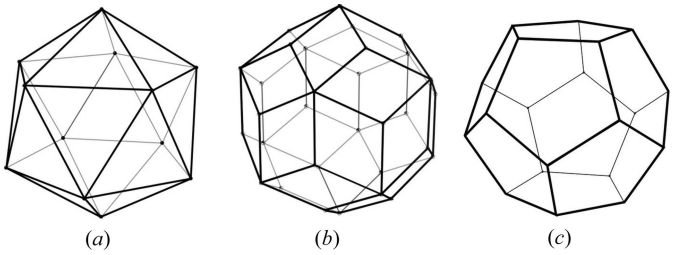

(*a*) (*b*) (*c*)

Figure 1
(*a*) Platonian icosahedron – a solid with 20 faces of equilateral triangular shape and 12 vertices. It has six fivefold, ten threefold and 15 twofold symmetry axes and 15 symmetry planes. The non-crystallographic Laue class related to icosahedral symmetry is $m\bar{3}\bar{5}$. (*b*) Keplerian triacontahedron (KTH) – solid object with 30 golden rhombuses on faces and 32 vertices. It has the same symmetry elements as the icosahedron. (*c*) Keplerian dodecahedron – a polyhedron dual to a Platonian icosahedron.

dimensional subspace, called parallel or physical, *via* a certain window (also called the atomic surface or acceptance domain). This procedure is known as the cut-and-project method. Choosing a proper window allows the reconstruction of quasicrystalline symmetry. The window for PIT has the shape of a Keplerian triacontahedron (KTH, see Fig. 1*b*). The atomic structure is retrieved by modelling (subdividing) the window. The main advantage of the higher-dimensional approach is its mathematical simplicity. However, it considers atoms to be stretched to multidimensional objects in *n*D space, which has no direct physical meaning. Including such phenomena as structural defects may also not be straightforward in this approach (Kozakowski, 2007).

A commonly used way to model i-QCs within the higher-dimensional method is the cluster-based approach. The idea is to consider the hierarchical packing of atomic clusters. Here, the polyhedral shells are frequently used to build clusters. The cluster analysis was successfully applied to structure solution and refinement of many i-QCs, *e.g.* the binary i-Cd–Yb system (Takakura *et al.*, 2007). The clusters in this structure are centred at the so-called 12-fold vertices – a subset of PIT nodes (PIT is considered as a framework structure) (Takakura, 2008). For that reason the statistical approach based on PIT seems to be promising in terms of the structure refinement of the binary i-Cd–Yb.

The statistical approach developed by Wolny (1998*a*,*b*) allows the structure solution in physical space only. The average unit cell concept (AUC) is used as a basic idea behind this approach. The AUC is defined as a distribution of projections of atomic positions on the so-called reference lattice, which is periodic. The detailed theoretical description of the method can be found in Wolny (1998*a*), Kozakowski & Wolny (2010) and Wolny *et al.* (2011). The AUC concept was successfully applied to the structure characterization of decagonal quasicrystals in Al–Ni–Co (Kuczera *et al.*, 2011) and Al–Cu–*Me* (*Me* = Co, Rh, Ir) (Kuczera *et al.*, 2012) systems, also at high temperatures (Kuczera *et al.*, 2014).

In this paper the AUC concept is applied to derive the structure-factor formula for an icosahedral model structure based on PIT (with monoatomic and arbitrary decoration). First attempts to obtain the decoration scheme for i-QCs based on PIT were made by Strzałka & Wolny (2014). The diffraction pattern calculated using the structure-factor formula derived here is compared with the results obtained by other methods (higher-dimensional approach and numerical calculations considered as the 'reference' data).

2. Higher-dimensional description

2.1. Direct space

The periodic (cubic) arrangement of atoms in six-dimensional direct space $\mathbf{V}$ is now considered. The six-dimensional vector basis of the direct space $\mathbf{V}$ can be chosen as (Steurer & Deloudi, 2009)

$$\mathbf{d}_1 = \frac{1}{2a^*}\begin{pmatrix}0\\0\\1\\0\\0\\1\end{pmatrix}_{\mathbf{V}}, \quad \mathbf{d}_i = \frac{1}{2a^*}\begin{pmatrix}\sin\theta\cos\frac{2\pi i}{5}\\ \sin\theta\sin\frac{2\pi i}{5}\\ \cos\theta\\ -\sin\theta\cos\frac{4\pi i}{5}\\ -\sin\theta\sin\frac{4\pi i}{5}\\ -\cos\theta\end{pmatrix}_{\mathbf{V}},$$
$$i = 2,\ldots,6, \quad \theta = 2\,\mathrm{arctg}(1/\tau), \tag{1}$$

where a^* is a constant (set equal to 1 in further calculations). Both the space and its vector basis will be denoted in the same way throughout the paper.

The first three components of each vector $\mathbf{d}_i$ denoted as $\mathbf{d}_i^{\parallel}$ span a Platonian dodecahedron (Fig. 1*c*), pointing towards the centres of its six walls. They define a three-dimensional subspace – the so-called parallel space (or physical space, both terms will be used interchangeably in this paper). The last three components denoted as $\mathbf{d}_i^{\perp}$ span the so-called perpendicular space. The projections of 64 vertices of a six-dimensional hypercube (periodic unit cell in six dimensions) on the three-dimensional perpendicular subspace (*via* vector basis $\mathbf{d}_i^{\perp}$) give 32 vertices of KTH (Fig. 1*b*) – the window known for PIT.

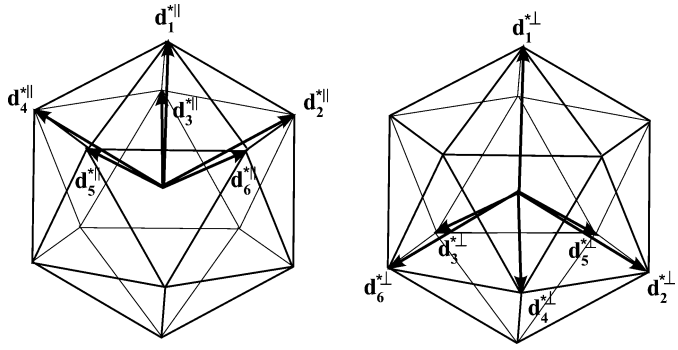

Figure 2
The reciprocal basis $\mathbf{V}^*$ of the six-dimensional hypercubic space. Components $\mathbf{d}_i^{*\parallel}$ span the three-dimensional parallel subspace and $\mathbf{d}_i^{*\perp}$ span the three-dimensional perpendicular one. Basis $\mathbf{V}^*$ describes well the icosahedral symmetry (in particular fivefold axes).

Table 1
Basis vectors $\mathbf{b}_i^*$ components and lengths.

Symbols '$\parallel$' and '$\perp$' refer to the parallel and perpendicular subspace, respectively. A simple identity $\tau = 2\cos(\pi/5)$ was used in equations (3) and (4).

Basis vectors	$\mathbf{b}_i^{*\parallel}$	$\mathbf{b}_i^{*\perp}$	Length	
			$b_i^{*\parallel} = \lvert\mathbf{b}_i^{*\parallel}\rvert$	$b_i^{*\perp} = \lvert\mathbf{b}_i^{*\perp}\rvert$
$\mathbf{b}_1^*$	$\frac{1}{4}\sin\theta[2\tau-1;\,(2-\tau)(\tau+2)^{1/2};\,0]$	$\frac{1}{4}\sin\theta[2\tau-1;\,(2-\tau)(\tau+2)^{1/2};\,0]$	$\frac{2}{(\tau+2)^{1/2}}\sin\theta \simeq 0.526$	$\frac{2\tau}{(\tau+2)^{1/2}}\sin\theta \simeq 0.851$
$\mathbf{b}_2^*$	$\frac{1}{4}\sin\theta[\tau+2;\,(\tau-1)(\tau+2)^{1/2};\,0]$	$\frac{1}{4}\sin\theta[\tau-3;\,-(\tau+2)^{1/2};\,0]$	$\frac{2\tau}{(\tau+2)^{1/2}}\sin\theta \simeq 0.851$	$\frac{2}{(\tau+2)^{1/2}}\sin\theta \simeq 0.526$
$\mathbf{b}_3^*$	$\frac{1}{4}[-(\tau-1)\sin\theta;\,(\tau+2)^{1/2}\sin\theta;\,2-2\cos\theta]$	$\frac{1}{4}[-\tau\sin\theta;\,-(\tau-1)(\tau+2)^{1/2}\sin\theta;\,2+2\cos\theta]$	$\frac{2}{(\tau+2)^{1/2}}\sin\theta \simeq 0.526$	$\frac{2\tau}{(\tau+2)^{1/2}}\sin\theta \simeq 0.851$
$\mathbf{b}_4^*$	$\frac{1}{4}[-\sin\theta;\,\tau(\tau+2)^{1/2}\sin\theta;\,2\cos\theta]$	$\frac{1}{4}[\sin\theta;\,-\tau(\tau+2)^{1/2}\sin\theta;\,-2\cos\theta]$	$\frac{2\tau}{(\tau+2)^{1/2}}\sin\theta \simeq 0.851$	$\frac{2}{(\tau+2)^{1/2}}\sin\theta \simeq 0.526$
$\mathbf{b}_5^*$	$\frac{1}{4}[(2-\tau)\sin\theta;\,-(\tau-1)(\tau+2)^{1/2}\sin\theta;\,2\cos\theta]$	$\frac{1}{4}[-(\tau+1)\sin\theta;\,-(\tau+2)^{1/2}\sin\theta;\,-2\cos\theta]$	$\frac{2}{(\tau+2)^{1/2}}\sin\theta \simeq 0.526$	$\frac{2\tau}{(\tau+2)^{1/2}}\sin\theta \simeq 0.851$
$\mathbf{b}_6^*$	$\frac{1}{4}[(\tau-1)\sin\theta;\,-(\tau+2)^{1/2}\sin\theta;\,2+2\cos\theta]$	$\frac{1}{4}[\tau\sin\theta;\,(\tau-1)(\tau+2)^{1/2}\sin\theta;\,2-2\cos\theta]$	$\frac{2\tau}{(\tau+2)^{1/2}}\sin\theta \simeq 0.851$	$\frac{2}{(\tau+2)^{1/2}}\sin\theta \simeq 0.526$

2.2. Reciprocal space – indexing scheme for diffraction pattern

The diffraction pattern is a reciprocal-space image of the structure. The relation of the reciprocal and direct basis is simply

$$\mathbf{d}_i\mathbf{d}_j^* = \delta_{ij}, \tag{2}$$

where $\mathbf{d}_j^*$ $(j = 1, \ldots, 6)$ is the set of basis vectors of six-dimensional reciprocal space $\mathbf{V}^*$ and δ_{ij} is the Kronecker delta. The explicit form of basis $\mathbf{V}^*$ is

$$\mathbf{d}_1^* = a^*\begin{pmatrix}0\\0\\1\\0\\0\\1\end{pmatrix}_{\mathbf{V}^*}, \quad \mathbf{d}_i^* = a^*\begin{pmatrix}\sin\theta\cos\frac{2\pi i}{5}\\ \sin\theta\sin\frac{2\pi i}{5}\\ \cos\theta\\ -\sin\theta\cos\frac{4\pi i}{5}\\ -\sin\theta\sin\frac{4\pi i}{5}\\ -\cos\theta\end{pmatrix}_{\mathbf{V}^*},$$
$$i = 2, \ldots, 6, \quad \theta = 2\,\mathrm{arctg}(1/\tau). \tag{3}$$

The basis $\mathbf{V}^*$ chosen as above reflects the icosahedral symmetry of the diffraction pattern. Parallel- and perpendicular-space components of basis $\mathbf{V}^*$ (defined analogously to the $\mathbf{V}$-space basis) span the vertices of a Platonian icosahedron (Fig. 2). Every diffraction peak can be indexed in the $\mathbf{V}^*$ basis using six integers. Also, another set of basis vectors can be used to define a reciprocal space, that is a set of six-dimensional Cartesian vectors $\mathbf{b}_i^*$ $(i = 1, \ldots, 6)$ of the reciprocal-space basis $\mathbf{B}^*$. The relation between the two basis vector sets is given by the following transformation (vectors $\mathbf{b}_i^*$ and $\mathbf{d}_i^*$ are column vectors) (Steurer & Deloudi, 2009):

$$\begin{pmatrix}\mathbf{b}_1^*\\ \mathbf{b}_2^*\\ \mathbf{b}_3^*\\ \mathbf{b}_4^*\\ \mathbf{b}_5^*\\ \mathbf{b}_6^*\end{pmatrix}_{\mathbf{B}^*} = \frac{1}{2}\begin{pmatrix}0 & \overline{1} & 0 & 0 & 0 & 1\\ 0 & 0 & \overline{1} & 0 & 1 & 0\\ 1 & 0 & 0 & \overline{1} & 0 & 0\\ 0 & 1 & 0 & 0 & 0 & 1\\ 0 & 0 & 1 & 0 & 1 & 0\\ 1 & 0 & 0 & 1 & 0 & 0\end{pmatrix}\begin{pmatrix}\mathbf{d}_1^*\\ \mathbf{d}_2^*\\ \mathbf{d}_3^*\\ \mathbf{d}_4^*\\ \mathbf{d}_5^*\\ \mathbf{d}_6^*\end{pmatrix}_{\mathbf{V}^*}$$
$$= \frac{1}{2}\begin{pmatrix}\mathbf{d}_6^* - \mathbf{d}_2^*\\ \mathbf{d}_5^* - \mathbf{d}_3^*\\ \mathbf{d}_1^* - \mathbf{d}_4^*\\ \mathbf{d}_6^* + \mathbf{d}_2^*\\ \mathbf{d}_5^* + \mathbf{d}_3^*\\ \mathbf{d}_1^* + \mathbf{d}_4^*\end{pmatrix}_{\mathbf{V}^*} \tag{4}$$

and the graphical interpretation is shown in Fig. 3.

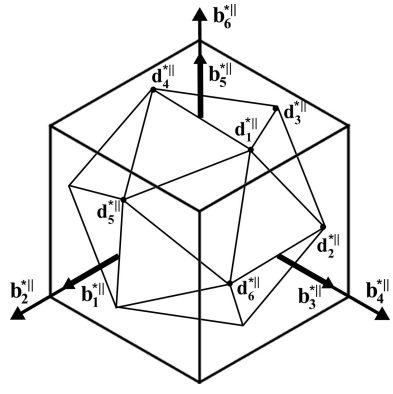

Figure 3
The relation between 'icosahedral' basis $\mathbf{V}^*$ and Cartesian basis $\mathbf{B}^*$ of the reciprocal space – parallel components. The ends of vectors $\mathbf{d}_i^{*\parallel}$ are marked with full circles. Vectors $\mathbf{b}_i^{*\parallel}$ with even indices are τ-times larger than those with odd indices. The origin for both $\mathbf{V}^*$ and $\mathbf{B}^*$ is the centre of an icosahedron.

Some features of vectors $\mathbf{b}_i^*$ important for the next paragraphs are discussed below. First, Table 1 shows the coordinates of vectors $\mathbf{b}_i^*$ in expanded form.

An interesting dependence of parallel- and perpendicular-space components of vectors $\mathbf{b}_i^*$ arises. Parallel-space vectors $\mathbf{b}_2^{*\parallel}, \mathbf{b}_4^{*\parallel}, \mathbf{b}_6^{*\parallel}$ are τ-times larger than $\mathbf{b}_1^{*\parallel}, \mathbf{b}_3^{*\parallel}, \mathbf{b}_5^{*\parallel}$, whereas vectors $\mathbf{b}_2^{*\perp}, \mathbf{b}_4^{*\perp}, \mathbf{b}_6^{*\perp}$ are τ-times smaller and have the opposite sign with respect to $\mathbf{b}_1^{*\perp}, \mathbf{b}_3^{*\perp}, \mathbf{b}_5^{*\perp}$. Moreover, the vectors have the same lengths within the above-mentioned triplets. The contents of Table 1 can be simplified as follows:

$$\begin{aligned} \mathbf{b}_{2,4,6}^{*\parallel} &= \tau \mathbf{b}_{1,3,5}^{*\parallel} \qquad b_{2,4,6}^{*\parallel} = \tau b_{1,3,5}^{*\parallel} = \frac{2\tau}{(\tau+2)^{1/2}} \sin\theta \simeq 0.851, \\ \mathbf{b}_{2,4,6}^{*\perp} &= -\tfrac{1}{\tau}\mathbf{b}_{1,3,5}^{*\perp} \qquad b_{2,4,6}^{*\perp} = \frac{1}{\tau} b_{1,3,5}^{*\perp} = \frac{2}{(\tau+2)^{1/2}} \sin\theta \simeq 0.526. \end{aligned} \tag{5}$$

The indexing scheme may now be expressed in basis $\mathbf{B}^*$. Every diffraction peak can be described by a reciprocal-space vector $\mathbf{G} = [\mathbf{k}, \mathbf{k}^\perp]$ (in six-dimensional reciprocal space):

$$\begin{aligned} \mathbf{k} &= (h_1 + \tau h_2)\mathbf{b}_1^{*\parallel} + (h_3 + \tau h_4)\mathbf{b}_3^{*\parallel} + (h_5 + \tau h_6)\mathbf{b}_5^{*\parallel}, \\ \mathbf{k}^\perp &= (h_2 - \tau h_1)\mathbf{b}_1^{*\perp} + (h_4 - \tau h_3)\mathbf{b}_3^{*\perp} + (h_6 - \tau h_5)\mathbf{b}_5^{*\perp}, \end{aligned} \tag{6}$$

where $h_1, \ldots, h_6$ are diffraction peak indices (integers). The property in relation (5) was used. For convenience, the sign '$\parallel$' was omitted for the parallel-space vector $\mathbf{k}$.

It is worth mentioning that the transformation (4) is linear. As a result, the direct-space basis $\mathbf{B}$ corresponding to the new setting of reciprocal basis $\mathbf{B}^*$ (vectors $\mathbf{b}_i^*$) also transforms linearly with $\mathbf{V}$. This means that the shape of a window in basis $\mathbf{B}$ is also given by a triacontahedral shape, but linearly transformed (rotated and scaled). The Cartesian basis setting will be useful in the next paragraphs for derivation of the reference lattice and AUC for PIT.

3. Average unit cell approach

To construct the AUC a reference lattice is needed. It must be periodic in three-dimensional parallel space. It is known (Wolny, 1998*a*) that for quasicrystalline structures one needs to use two reference lattices, for which the lattice parameters differ by a factor τ. The positions of every node of PIT can be expressed using the reference lattice constants as follows:

$$\begin{aligned} x &= \alpha_1 \lambda_{k1} + u_x \qquad x = \beta_1 \lambda_{q1} + v_x \\ y &= \alpha_2 \lambda_{k2} + u_y \qquad y = \beta_2 \lambda_{q2} + v_y \\ z &= \alpha_3 \lambda_{k3} + u_z \qquad z = \beta_3 \lambda_{q3} + v_z \end{aligned} \tag{7}$$

where x, y, z are the physical-space positions of PIT nodes; $\lambda_{ki}, \lambda_{qi}$ $(i = 1, 2, 3)$ are the lattice constants in three directions for two reference lattices associated with the subscripts k and q; α_i, β_i $(i = 1, 2, 3)$ are integers; $u_x, u_y, u_z, v_x, v_y, v_z$ are remainder components of the projections of PIT positions onto the reference lattices with respect to the nearest nodes (new positions of PIT in the reference lattice), and their values vary from 0 to λ_{ki} or λ_{qi}, respectively.

The AUC is the distribution $P(u_x, u_y, u_z, v_x, v_y, v_z)$ of projections of PIT nodes on the reference lattices. The lattice constants can be, in general, arbitrarily chosen. However, it is reasonable to associate them with the set of reciprocal-space vectors used for indexing the diffraction pattern. Let us then write

$$\lambda_{ki} = \frac{2\pi}{k_{0i}}; \quad \lambda_{qi} = \frac{2\pi}{q_{0i}}; \quad i = 1, 2, 3, \tag{8}$$

where k_{0i}, q_{0i} are the lengths of $\mathbf{k}_{0i}, \mathbf{q}_{0i}$ $(i = 1, 2, 3)$ used for indexing in reciprocal parallel space (the index '$\parallel$' in the superscript is omitted). Since we choose $\lambda_{ki} = \tau\lambda_{qi}$, vectors $\mathbf{q}_{0i} = (1/\tau)\mathbf{k}_{0i}$ are called modulation vectors, whereas $\mathbf{k}_{0i}$ are reciprocal-space vectors. The τ relation used here is typical for this type of quasicrystal.

For convenience, the orthogonal set of vectors $\mathbf{k}_{0i}$ and $\mathbf{q}_{0i}$ is expected. Therefore, Cartesian basis $\mathbf{B}^*$ [see equation (5)] can be used to construct the reference lattices. We define vectors $\mathbf{k}_{0i}, \mathbf{q}_{0i}$ as parallel to vectors $\mathbf{b}_i^{*\parallel}$ with shorter lengths $b_i^{*\parallel}/\sin\theta$ and rescaled by 2π. Analogously, as their perpendicular-space counterparts $\mathbf{k}_{0i}^\perp, \mathbf{q}_{0i}^\perp$, rescaled vectors $\mathbf{b}_i^{*\perp}$ will be used. The τ relation between reciprocal-space and modulation vectors is preserved due to the properties of vectors $\mathbf{b}_i^*$ discussed in §2.2. The vector basis chosen for further consideration within the statistical approach is presented below (for comparison, see Table 1):

$$\begin{array}{lll} \mathbf{q}_{01} = [q_0, 0, 0]; & \mathbf{q}_{02} = [0, q_0, 0]; & \mathbf{q}_{03} = [0, 0, q_0] \\ \mathbf{q}_{01}^\perp = [-q_0^\perp, 0, 0]; & \mathbf{q}_{02}^\perp = [0, -q_0^\perp, 0]; & \mathbf{q}_{03}^\perp = [0, 0, -q_0^\perp] \\ \mathbf{k}_{01} = [k_0, 0, 0]; & \mathbf{k}_{02} = [0, k_0, 0]; & \mathbf{k}_{03} = [0, 0, k_0] \\ \mathbf{k}_{01}^\perp = [k_0^\perp, 0, 0]; & \mathbf{k}_{02}^\perp = [0, k_0^\perp, 0]; & \mathbf{k}_{03}^\perp = [0, 0, k_0^\perp] \end{array} \tag{9}$$

where $q_0 = k_0^\perp = 2\pi/(\tau+2)^{1/2}$, $q_0^\perp = k_0 = 2\pi\tau/(\tau+2)^{1/2}$. The Cartesian coordinate system is used.

The six-dimensional reciprocal-space vector $\mathbf{G}$ [equation (6)] must be redefined as follows:

$$\begin{aligned} \mathbf{k} &= h_1\mathbf{q}_{01} + h_2\mathbf{k}_{01} + h_3\mathbf{q}_{02} + h_4\mathbf{k}_{02} + h_5\mathbf{q}_{03} + h_6\mathbf{k}_{03} \\ &= (h_1 + \tau h_2)\mathbf{q}_{01} + (h_3 + \tau h_4)\mathbf{q}_{02} + (h_5 + \tau h_6)\mathbf{q}_{03} \\ \mathbf{k}^\perp &= h_1\mathbf{k}_{01}^\perp + h_2\mathbf{q}_{01}^\perp + h_3\mathbf{k}_{02}^\perp + h_4\mathbf{q}_{02}^\perp + h_5\mathbf{k}_{03}^\perp + h_6\mathbf{q}_{03}^\perp \\ &= (h_2 - \tau h_1)\mathbf{q}_{01}^\perp + (h_4 - \tau h_3)\mathbf{q}_{02}^\perp + (h_6 - \tau h_5)\mathbf{q}_{03}^\perp. \end{aligned} \tag{10}$$

Formally, the indices $h_1, \ldots, h_6$ used in (10) are not equivalent with those in (6), but it is not relevant.

3.1. Properties of the AUC

In this section we show important properties of the AUC for PIT. Let us consider the six-dimensional definition of reciprocal space:

$$\exp(i\mathbf{G}\cdot\mathbf{R}) = 1, \tag{11}$$

where $\mathbf{R}$ is the position of a node of PIT in six-dimensional hyperspace and $\mathbf{G}$ is the six-dimensional reciprocal-space vector, as previously. $\mathbf{R} = [\mathbf{r}^\parallel, \mathbf{r}^\perp] = [x, y, z, x^\perp, y^\perp, z^\perp]$, where $\mathbf{r}^\parallel$ represents the physical-space position of a point in PIT and $\mathbf{r}^\perp$ stands for a position in the window (perpendicular space). Considering relations (9) and (10) we can write

$$\mathbf{G}\cdot\mathbf{R}=\sum_{i=1,3,5}h_i\left(\mathbf{q}_{0i}\mathbf{r}^{\parallel}+\mathbf{q}_{0i}^{\perp}\mathbf{r}^{\perp}\right)+\sum_{j=2,4,6}h_j\left(\mathbf{k}_{0j}\mathbf{r}^{\parallel}+\mathbf{k}_{0j}^{\perp}\mathbf{r}^{\perp}\right). \quad (12)$$

For the components $\mathbf{r}^{\parallel}$ we can use the reference lattice system (7) and relation (8). The expressions from equation (12) in expanded form are

$$\begin{aligned}
h_1\mathbf{q}_{01}\cdot\mathbf{r}^{\parallel}&=h_1\left[q_0,0,0\right]\cdot[x,y,z]=h_1q_0x=h_1q_0\left(\beta_1\lambda_{q1}+v_x\right)\\
&=h_1q_0\left(\beta_1\frac{2\pi}{q_0}+v_x\right)=2\pi\beta_1h_1+h_1q_0v_x\\
h_2\mathbf{k}_{01}\cdot\mathbf{r}^{\parallel}&=h_2\left[k_0,0,0\right]\cdot[x,y,z]=h_2k_0x=h_2k_0(\alpha_1\lambda_{k1}+u_x)\\
&=h_2k_0\left(\alpha_1\frac{2\pi}{k_0}+u_x\right)=2\pi\alpha_1h_2+h_2k_0u_x\\
h_1\mathbf{q}_{01}^{\perp}\cdot\mathbf{r}^{\perp}&=h_1\left[-q_0^{\perp},0,0\right]\cdot\left[x^{\perp},y^{\perp},z^{\perp}\right]=-h_1q_0^{\perp}x^{\perp}\\
h_2\mathbf{k}_{01}^{\perp}\cdot\mathbf{r}^{\perp}&=h_2\left[k_0^{\perp},0,0\right]\cdot\left[x^{\perp},y^{\perp},z^{\perp}\right]=h_2k_0^{\perp}x^{\perp}
\end{aligned} \quad (13)$$

and analogously for the rest of the components of the sum (12).

It is easy to see that terms like $2\pi\beta_1h_1$ or $2\pi\alpha_1h_2$ vanish in the exponent, since α_1,β_1,h_1,h_2 are integers. We can then rewrite (12) in the following form:

$$\begin{aligned}
\mathbf{G}\cdot\mathbf{R}=&h_1\left(q_0v_x-q_0^{\perp}x^{\perp}\right)+h_2\left(k_0u_x+q_0^{\perp}x^{\perp}\right)\\
&+h_3\left(q_0v_y-q_0^{\perp}y^{\perp}\right)+h_4\left(k_0u_y+k_0^{\perp}y^{\perp}\right)\\
&+h_5\left(q_0v_z-q_0^{\perp}z^{\perp}\right)+h_6\left(k_0u_z+k_0^{\perp}z^{\perp}\right).
\end{aligned} \quad (14)$$

The formula (11) is satisfied for any indices $h_1,\ldots,h_6$. The zeroing condition for (14) yields

$$\begin{aligned}
v_x&=\frac{q_0^{\perp}}{q_0}x^{\perp}=\tau x^{\perp} \quad u_x=-\frac{k_0^{\perp}}{k_0}x^{\perp}=-\frac{1}{\tau}x^{\perp}\\
v_y&=\frac{q_0^{\perp}}{q_0}y^{\perp}=\tau y^{\perp} \quad u_y=-\frac{k_0^{\perp}}{k_0}y^{\perp}=-\frac{1}{\tau}y^{\perp}.\\
v_z&=\frac{q_0^{\perp}}{q_0}z^{\perp}=\tau z^{\perp} \quad u_z=-\frac{k_0^{\perp}}{k_0}z^{\perp}=-\frac{1}{\tau}z^{\perp}
\end{aligned} \quad (15)$$

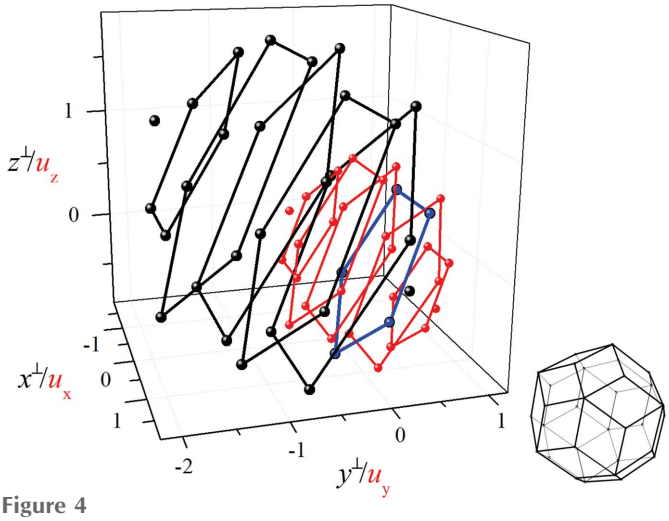

Figure 4
The window (black) in **B** basis and the AUC (red) for PIT. The 'skeleton' of KTHs (parallel layers spanned by five vertices) is shown for better comparison of shapes. The blue layer is common for both. It is easy to see that the two shapes are related by the scaling factor $-1/\tau$.

We obtained a proof that the shapes of distributions $P(u_x,u_y,u_z)$ and $P(v_x,v_y,v_z)$ are the same as the shapes of the window, *i.e.* the KTH, but linearly scaled [for more details on the shapes of the AUC for different basis vectors, see Strzalka *et al.* (2013)]. Fig. 4 presents graphically the results from (15).

Another important fact is that components v_i and $u_i\,(i=x,y,z)$ are not independent. Substituting $x^{\perp}$, $y^{\perp}$ and $z^{\perp}$ in the left triples of (15) with the ones obtained from the right gives

$$\begin{aligned}
v_x&=\frac{q_0^{\perp}}{q_0}x^{\perp}=\frac{q_0^{\perp}}{q_0}\left(-\frac{k_0}{k_0^{\perp}}\right)u_x=-\tau^2u_x\\
v_y&=\frac{q_0^{\perp}}{q_0}y^{\perp}=\frac{q_0^{\perp}}{q_0}\left(-\frac{k_0}{k_0^{\perp}}\right)u_y=-\tau^2u_y\\
v_z&=\frac{q_0^{\perp}}{q_0}z^{\perp}=\frac{q_0^{\perp}}{q_0}\left(-\frac{k_0}{k_0^{\perp}}\right)u_z=-\tau^2u_z
\end{aligned} \quad (16)$$

where the relations (9) were used.

Relation (16) means that the full distribution $P(u_x,u_y,u_z,v_x,v_y,v_z)$ is non-zero only for segment lines $v_i=-\tau^2u_i$. This scaling property reduces the dimensionality of the AUC to 3. It is known in the literature as TAU2 scaling (Wolny *et al.*, 2013). Since (16) is known, the marginal distribution $P(u_x,u_y,u_z)$ itself will be considered as the AUC in further steps.

3.2. Numerical derivation of the AUC

The numerical calculations confirm all analytical results obtained in §3.1. In the following sequence of pictures one can see about 200 000 points of the AUC calculated numerically. From Fig. 5(*a*) we conclude that in both cases the AUC shape is given by KTH. More detailed analysis is shown in Figs. 5(*b*), 5(*c*). Numerical calculations also confirm the characteristic scaling in the $v_i(u_i)$ relation (Fig. 6).

4. Diffraction pattern

The diffraction pattern for PIT consists of sharp peaks. Their intensities can be calculated as the squared modulus of the structure factor (we consider a purely geometrical definition of the structure factor). The structure factor is the Fourier transform of atomic positions in a crystal structure:

$$F(\mathbf{k})=\sum_j f_j\exp\left(i\mathbf{k}\cdot\mathbf{r}_j^{\parallel}\right), \quad (17)$$

where $\mathbf{k}$ is the reciprocal vector in physical space [the parallel component of the six-dimensional vector $\mathbf{G}$, see (10)], $\mathbf{r}^{\parallel}$ is the position of the jth atom and f_j is an atomic form factor of atom j. For simplicity, in further derivation all decorating atoms are considered to be the same and their form factors are set to 1. The atomic arrangement in physical space is not known, the idea would be to model the structure in perpendicular space (higher-dimensional approach). Considering (11) and (12),

$$\mathbf{G}\cdot\mathbf{R}=\mathbf{k}\cdot\mathbf{r}^{\parallel}+\mathbf{k}^{\perp}\cdot\mathbf{r}^{\perp}=0\ \rightarrow\ \mathbf{k}\cdot\mathbf{r}^{\parallel}=-\mathbf{k}^{\perp}\cdot\mathbf{r}^{\perp} \quad (18)$$

and the formula (17) turns into

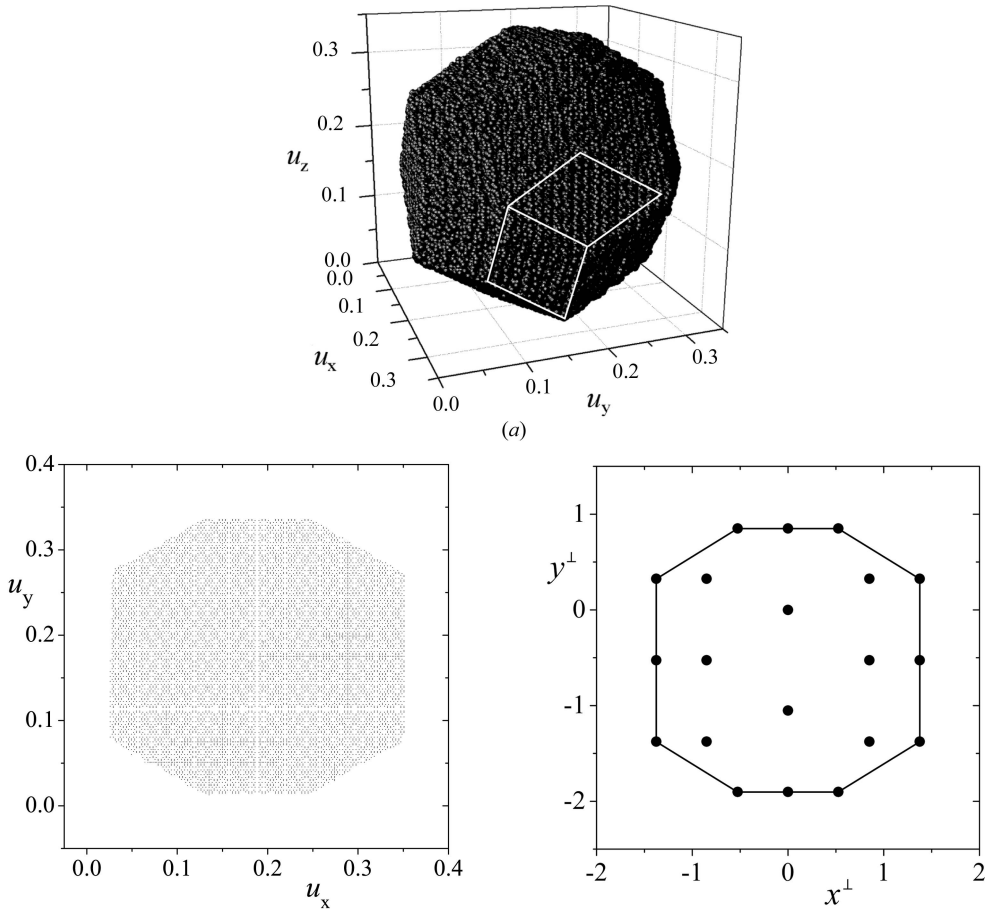

Figure 5
(*a*) Numerically obtained 200 000 points of the AUC calculated for a reference lattice constructed with vectors given by (9). The shape of the AUC is KTH (two selected golden rhombuses as facets marked with a red contour). *XY* projections of numerically obtained AUC (*b*) and window (*c*) confirm the linear dependence of the two objects (the scale is not preserved). The AUC is a dense and uniform distribution of projected atomic positions.

$$F(\mathbf{k}) = \int_W \exp\left(-i\mathbf{k}^\perp \cdot \mathbf{r}^\perp\right) \mathrm{d}^3\mathbf{r}^\perp. \tag{19}$$

Because we deal with a dense and continuous distribution of points in perpendicular space, summation in (17) can be replaced by integration limited to the shape of a window (W).

4.1. The structure factor within the AUC approach

The structure factor can also be expressed in physical space using the statistical approach. The exponent in (17) can be written in physical space by using (7) and based on the discussion in §3.1. Moreover, applying (15) and (16) gives

$$\begin{aligned}\mathbf{k}\cdot\mathbf{r}^{\parallel} &= h_1q_0v_x + h_2k_0u_x + h_3q_0v_y + h_4k_0u_y + h_5q_0v_z + h_6k_0u_z\\ &= h_1\frac{k_0}{\tau}\left(-\tau^2u_x\right) + h_2k_0u_x + h_3\frac{k_0}{\tau}\left(-\tau^2u_y\right) + h_4k_0u_y\\ &\quad + h_5\frac{k_0}{\tau}\left(-\tau^2u_z\right) + h_6k_0u_z\\ &= k_0\left[(h_2-\tau h_1)u_x + (h_4-\tau h_3)u_y + (h_6-\tau h_5)u_z\right].\end{aligned} \tag{20}$$

The structure-factor formula expressed in physical space reads

$$\begin{aligned}F(\mathbf{k}) &= \int_{\mathrm{AUC}} \exp(i\boldsymbol{\chi}\cdot\mathbf{u})\,\mathrm{d}^3\mathbf{u}\\ \boldsymbol{\chi} &= \left[\chi_x, \chi_y, \chi_z\right] = k_0\left[(h_2-\tau h_1); (h_4-\tau h_3); (h_6-\tau h_5)\right]\\ \mathbf{u} &= \left[u_x, u_y, u_z\right] = \left[-\frac{1}{\tau}x^\perp; -\frac{1}{\tau}y^\perp; -\frac{1}{\tau}z^\perp\right],\end{aligned} \tag{21}$$

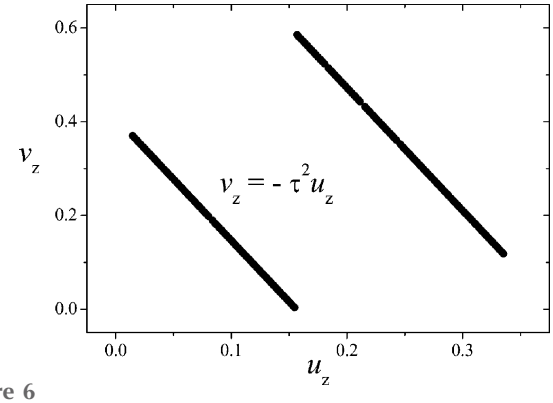

Figure 6
$v_z(u_z)$ plot related to the distribution $P(u_x, u_y, u_z, v_x, v_y, v_z)$ obtained numerically. The slope of the linear dependence is '$-\tau^2$', which perfectly confirms the theoretical prediction (18).

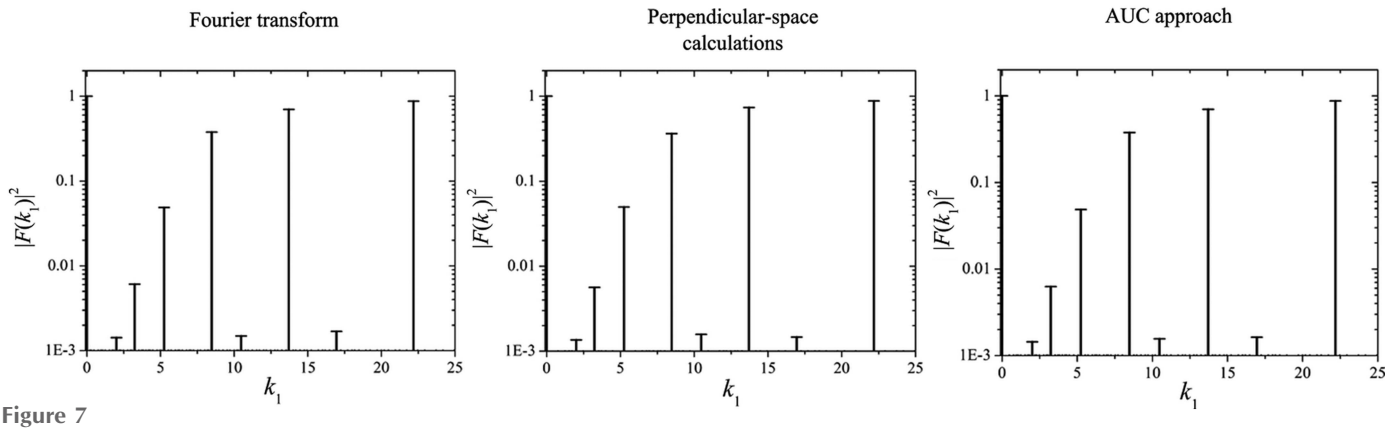

Figure 7
Diffraction pattern for reciprocal-space vector $\mathbf{k}_1$ obtained by using three methods as described in §4.2.

where $k_0 = 2\pi\tau/(\tau+2)^{1/2}$. The region of integration in (21) can be reduced to distribution $P(u_x, u_y, u_z)$ only. By definition, each position u_i is limited to the interval $(0, \lambda_{ki})$ [see formula (7)]. The structure factor finally gets the following form:

$$F(\mathbf{k}) = \int_0^{\lambda_{k1}} \int_0^{\lambda_{k2}} \int_0^{\lambda_{k3}} P(u_x, u_y, u_z) \exp(i\boldsymbol{\chi}\cdot\mathbf{u})\, \mathrm{d}^3\mathbf{u}, \qquad (22)$$

where $\lambda_{k1}, \lambda_{k2}, \lambda_{k3}$ are lattice constants for three directions of the reference lattice. Formula (22) can be even further simplified by taking into account relation (8).

4.2. Diffraction pattern for PIT

The diffraction pattern for PIT decorated in the lattice nodes has been derived in three different ways:

(i) Numerically, as a Fourier transform of a point set in three-dimensional physical space (atomic positions) – it plays the role of the reference data. About 2 million points of PIT were taken into account.

(ii) Theoretically, by analytical integration over the triacontahedral shape in perpendicular space [using (19)].

(iii) Within the statistical approach, by analytical integration over the triacontahedral shape of the AUC [using (22)].

To calculate the intensity of the diffraction peaks only a 'purely geometrical' term was used, *i.e.* $I = |F(\mathbf{k})|^2$. The obtained diffraction pattern has been presented for one-dimensional reciprocal-space vector $\mathbf{k}_1$. All peaks are normalized to '0' peaks (peaks at the position $k_1 = 0$). The logarithmic scale was used for more precise comparison. The results are shown in Fig. 7.

The patterns are identical, *i.e.* all peak positions are the same and the peak heights agree on all three graphs. In Fig. 8, the $|F_{\rm AUC}|^2/|F_{\rm num}|^2$ plot for about 10 000 selected peaks is shown. It is a correlation of data from statistical and numerical calculations. Perfect agreement is confirmed.

5. Arbitrarily decorated PIT

5.1. KTH subdivision

We proved numerically and analytically the relation between the AUC and the window shape (KTH in both cases). To obtain a decoration scheme we will consider a window subdivision by means of dividing the KTH into golden rhombohedra in the perpendicular subspace of the six-dimensional direct space. The structure-factor formula will however be derived within the AUC approach. It needs to be stressed that every rhombohedron (OR or AR) at a given orientation in physical space (where atomic arrangement is observed) corresponds to a certain rhombohedron (AR or OR, respectively) in perpendicular space.

There are ten orientations of ORs and ARs subdividing the Platonian icosahedron in three-dimensional reciprocal space (see Appendix *A*). The same stands for the perpendicular subspace (window) of six-dimensional direct space. For further considerations we have chosen two independent orientations of ORs and ARs which are spanned by basis vectors of the 'icosahedral' basis **V**: $\{\mathbf{d}_1^\perp, \mathbf{d}_2^\perp, \mathbf{d}_6^\perp\}$ – OR1, $\{\mathbf{d}_2^\perp, \mathbf{d}_6^\perp, -\mathbf{d}_4^\perp\}$ – OR2 and $\{\mathbf{d}_1^\perp, \mathbf{d}_3^\perp, \mathbf{d}_6^\perp\}$ – AR1, $\{\mathbf{d}_2^\perp, \mathbf{d}_6^\perp, -\mathbf{d}_5^\perp\}$ – AR2. The spanning vectors originate at the reference vertex, which plays the role of a label for each rhombohedron. The chosen orientations are equivalent with respect to fivefold rotation symmetry along the axis defined by vector $\mathbf{d}_6^\perp$ of basis **V**, called the 'z axis' from now on.

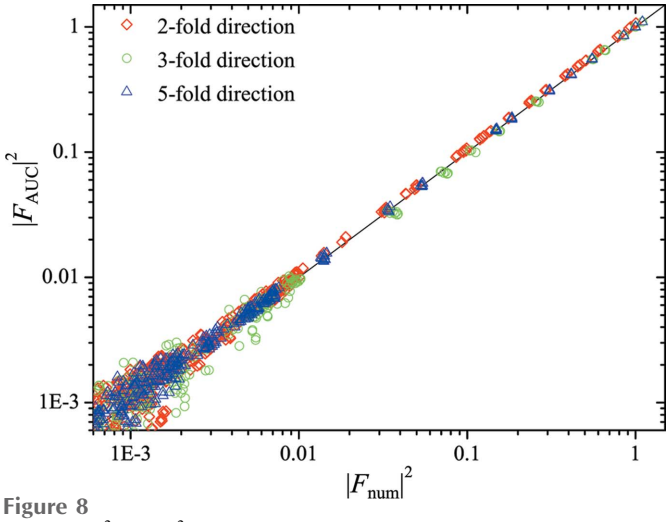

Figure 8
The $|F_{\rm AUC}|^2/|F_{\rm num}|^2$ plot for about 10 000 peaks at different directions of the wavevector (two-, three- and fivefold axes in reciprocal space).

Table 2
Analytical definition of vectors $\mathbf{e}_1, \mathbf{e}_2, \mathbf{e}_3$ spanning the subdomains for ORs and ARs in perpendicular space.

Basis **V** is used. Subdomains for OR2 and AR2 are shifted from the origin of the coordinate system.

	Reference vertex O	$\mathbf{e}_1$	$\mathbf{e}_2$	$\mathbf{e}_3$
OR1	Origin	$\mathbf{d}_3^\perp$	$\mathbf{d}_5^\perp$	$\mathbf{d}_4^\perp$
OR2	$\mathbf{d}_1^\perp + \mathbf{d}_4^\perp$	$\mathbf{d}_3^\perp$	$\mathbf{d}_5^\perp$	$-\mathbf{d}_1^\perp$
AR1	Origin	$\mathbf{d}_2^\perp$	$\mathbf{d}_4^\perp$	$\mathbf{d}_5^\perp$
AR2	$\mathbf{d}_1^\perp + \mathbf{d}_5^\perp$	$\mathbf{d}_3^\perp$	$-\mathbf{d}_1^\perp$	$\mathbf{d}_4^\perp$

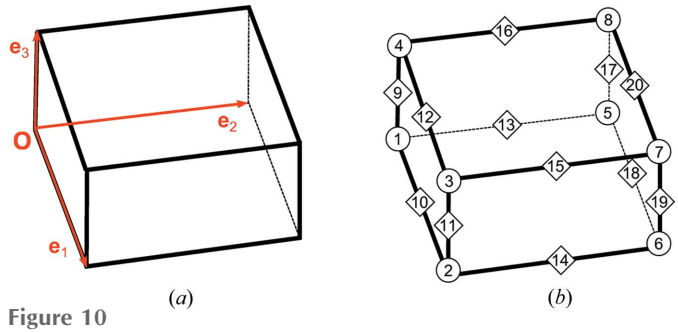

Figure 10
(*a*) Vectors $\mathbf{e}_1$, $\mathbf{e}_2$, $\mathbf{e}_3$ (in red) spanning OR in perpendicular space. (*b*) Characteristic positions in rhombohedra in physical space: numbers on edges (in squares) and vertices (in circles) correspond to Table 3.

Shifting rhombohedra in physical space causes a shift of corresponding rhombohedra in perpendicular space. By applying a simple condition that the vertices of any rhombohedron in any given orientation must be located inside the window in perpendicular space, the distributions of reference vertices are obtained (for the results of numerical derivation see Fig. 9). Such distributions in perpendicular space will be called subdomains. They are the fundamental units of the subdivision scheme. The distributions of reference vertices belonging to ORs (ARs) cut out from the KTH subdomains in the shape of acute (obtuse) golden rhombohedra. After applying the fivefold symmetry we find the entire subdivision scheme of KTH into 20 independent rhombohedral subdomains (Fig. 9).

The subdomains can also be defined analytically using direct-space basis vectors. Table 2 shows the definition of

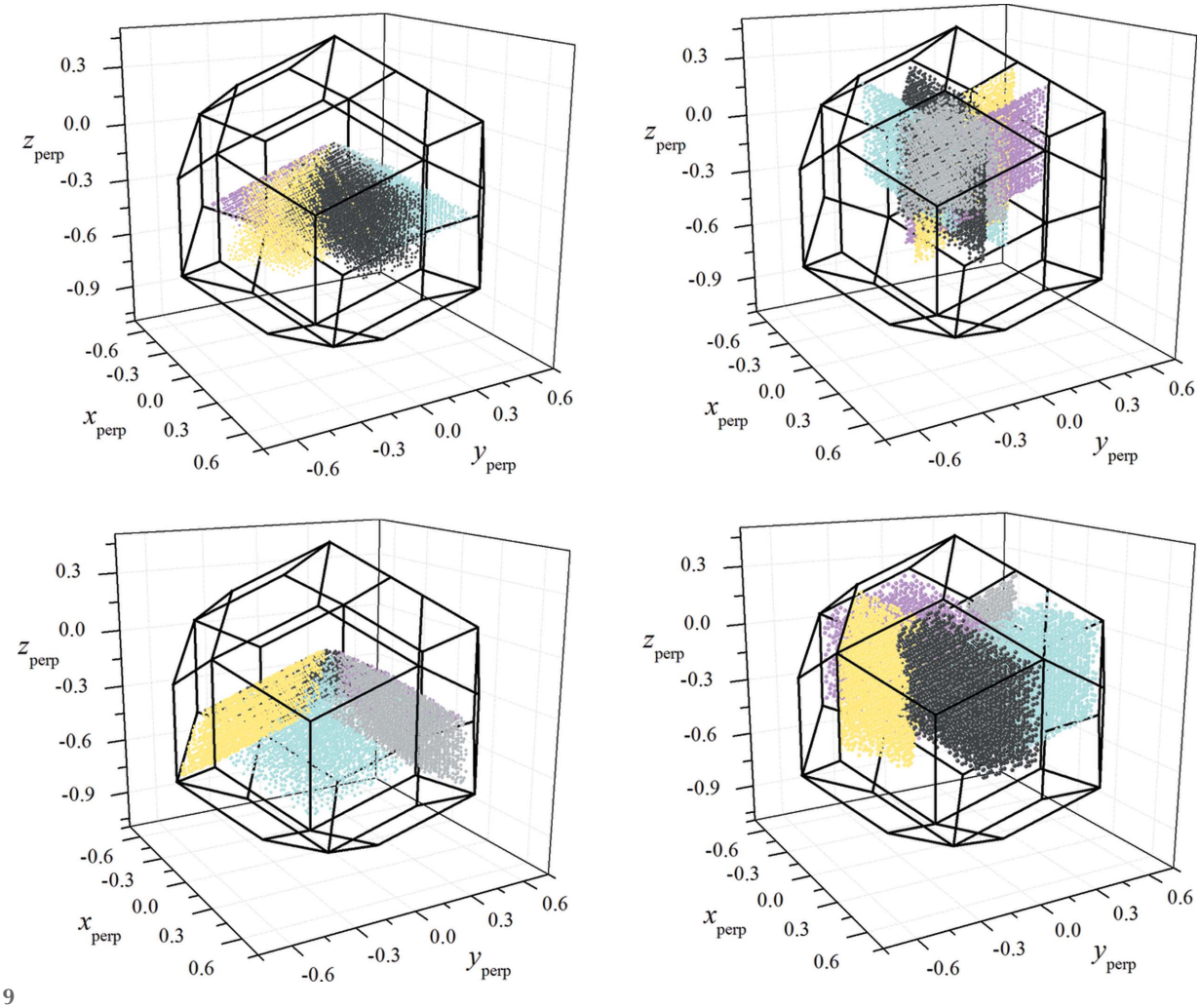

Figure 9
Subdomains in perpendicular space understood as position distribution of the reference vertices of the structural units: ORs (upper) and ARs (lower images).

vectors $\mathbf{e}_1, \mathbf{e}_2, \mathbf{e}_3$ spanning the rhombohedral subdomains at basic orientations and their reference vertices (see Fig. 10*a*). Coordinates for other orientations can be obtained by rotation along the 'z axis' by an angle of $4\pi/5$.

5.2. Structure-factor formula in the case of arbitrary decoration

To derive the formula for the structure factor one has to calculate the Fourier transform of each subdomain. Integration can be carried out in the oblique coordinates related to vectors $\mathbf{e}_1, \mathbf{e}_2, \mathbf{e}_3$. The Fourier transform of subdomains in a given orientation l reads

$$F_l^{\mathrm{OR/AR}}(\mathbf{k}) = \int \exp\left(-i\mathbf{k}^{\perp}\mathbf{r}^{\perp}\right) \mathrm{d}^3\mathbf{r}^{\perp} = V \int_{X_O}^{X} \mathrm{d}x \int_{Y_O}^{Y} \mathrm{d}y \int_{Z_O}^{Z} \exp\left[-i(q_1 x + q_2 y + q_3 z)\right] \mathrm{d}z, \tag{23}$$

where $q_j = \mathbf{k}^{\perp}\mathbf{e}_j$, $j \in \{1, 2, 3\}$, $\mathbf{e}_j$, $j \in \{1, 2, 3\}$ are vectors spanning the subdomains defined as in Fig. 10(*a*), $\mathbf{r}^{\perp} = x\mathbf{e}_1 + y\mathbf{e}_2 + z\mathbf{e}_3$, $V = |\mathbf{e}_1(\mathbf{e}_2 \times \mathbf{e}_3)|$ is the volume of a subdomain spanned by vectors $\mathbf{e}_1, \mathbf{e}_2, \mathbf{e}_3$. X, Y, Z are coordinates of the vertices of subdomains defined as in Fig. 10(*a*) in the oblique reference system (*i.e.* the lengths of vectors $\mathbf{e}_1, \mathbf{e}_2, \mathbf{e}_3$; see Table 2), and X_O, Y_O, Z_O are coordinates of the reference vertices of subdomains (see Table 2).

The exact results of analytical integration in (23) for eight different cases of q_j values can be found in Appendix *B*.

As a last step we need to find the fraction of an atom inside the structural unit (denoted as α_j for atom j). For atoms placed on the faces of ORs or ARs: $\alpha_j = 1/2$. Fraction α_j for an atom located on the edge is equal to $\gamma/2\pi$, where γ is a plane angle between faces adjacent to this edge. In the last case – an atom located on a vertex – the fraction is defined as $\Omega/4\pi$, where Ω is a solid angle between edges meeting at the considered vertex. The angle Ω can be calculated with a formula given in van Oosterom & Strackee (1983):

$$\tan\left(\frac{\Omega}{2}\right) = \frac{\left|(\mathbf{a} \times \mathbf{b}) \cdot \mathbf{c}\right|}{abc + (\mathbf{a} \cdot \mathbf{b})c + (\mathbf{a} \cdot \mathbf{c})b + (\mathbf{b} \cdot \mathbf{c})a}, \tag{24}$$

where $\mathbf{a}, \mathbf{b}, \mathbf{c}, a, b, c$ are vectors determining a vertex and their lengths.

Table 3 shows fractions calculated as discussed above.

The subdivision scheme for the shape of the AUC is the same as derived in §5.1. Similarly, the Fourier transforms of subdomains as defined in (23) can be expressed within the statistical method. Based on the discussion in §§5.1 and 5.2 we are finally able to derive a full structure-factor formula for arbitrarily decorated structural units of PIT within the statistical approach:

$$F(\boldsymbol{\chi}) = \sum_{l=1}^{10}\left[F(\boldsymbol{\chi})_l^{\mathrm{OR}} \sum_{j=1}^{N_1} f_j \alpha_j \exp(i\mathbf{k} \cdot \mathbf{r}_j^l)\right] + \sum_{l=1}^{10}\left[F(\boldsymbol{\chi})_l^{\mathrm{AR}} \sum_{j=1}^{N_2} f_j \alpha_j \exp(i\mathbf{k} \cdot \mathbf{r}_j^l)\right], \tag{25}$$

Table 3
Fractions α_j of atoms decorating structural units.

The numbers in the first row are labels of the characteristic locations in the unit as defined in Fig. 10(*b*).

	1, 7	2, 3, 5, 8	4, 6	9, 19	10, 13, 15, 20	11, 17	12, 14, 16, 18
OR	0.05	0.15	0.15	0.2	0.2	0.3	0.3
AR	0.05	0.05	0.35	0.4	0.1	0.1	0.4

where $\boldsymbol{\chi} = k_0[(h_2 - h_1\tau), (h_4 - h_3\tau), (h_6 - h_5\tau)]$, $h_1, \ldots, h_6$ are integer indices, and N_1, N_2 are the number of atoms decorating ORs and ARs, respectively. $F(\boldsymbol{\chi})_l^{\mathrm{OR}}/F(\boldsymbol{\chi})_l^{\mathrm{AR}}$ is the Fourier transform of the subdomain related to OR/AR at a given orientation l in physical space, f_j the atomic form factor of the jth atom, α_j the fraction of the jth atom decorating the structural unit, and $\mathbf{r}_j^l$ the position of atom j in the structure unit with respect to a reference vertex.

$F(\boldsymbol{\chi})_l^{\mathrm{OR}}$, $F(\boldsymbol{\chi})_l^{\mathrm{AR}}$ are calculated using formula (23) under constraints given in Table 2 within the statistical approach. Such calculations are consistent with the ones performed in perpendicular space, as proved in §4.2.

The diffraction pattern along five-, three- and twofold symmetry axes was calculated using formula (25). For the reason of complexity of possible decoration schemes for i-QCs, the simplest case of monoatomic decoration at the vertices of rhombohedra was considered. Peak intensities ($I = |F(\boldsymbol{\chi})|^2$) have been compared with corresponding ones calculated numerically over 77 000 points of PIT in the log–log plot (Fig. 11). All peaks with indices ranging from −5 to 5 appearing in the diffraction pattern are included. The correctness of the obtained structure factor (25) is fully confirmed for that simple case.

6. Conclusions

The comprehensive description of the statistical method applied to primitive icosahedral tiling as a model of an icosahedral quasicrystal was introduced in this paper. The

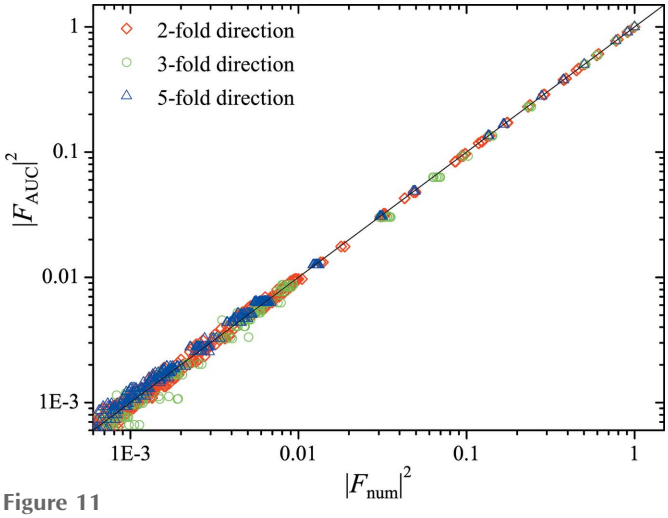

Figure 11
Correlation between peak intensities calculated numerically and using formula (25).

average unit cell concept was used for derivation of the structure factor. In the first part, the application of the statistical method to PIT was shown with all mathematical details and the structure factor for monoatomic decoration was derived. All calculations were made in three-dimensional physical space in contrast to the higher-dimensional method. It was shown that, for a proper choice of vectors spanning the reference lattice, the shape of the AUC is exactly the same as that of the window constructed in perpendicular space within the cut-and-project method. The diffraction patterns obtained in three different ways (numerically, higher-dimensional analysis and statistical description) were compared. Full agreement of patterns was shown, which proves the correctness of the statistical approach and its equivalence to the higher-dimensional method. Our approach, however, has the advantage of enabling the calculation in physical space.

In the second part, the structure-factor formula for arbitrarily decorated PIT (atoms placed in the vertices, edges or inside the structural units) was derived. For this purpose, a subdivision scheme of a window in perpendicular space (equivalent to subdivision of the AUC) was introduced in detail. This results in a definition of 20 symmetrically inequivalent subdomains dividing the Keplerian triacontahedra. Each of them represents a certain orientation of obtuse or acute golden rhombohedra considered as structure units of PIT and filling the three-dimensional physical space in an aperiodic way with icosahedral symmetry. The complete structure-factor formula (25) was derived in physical space within the AUC approach. The information about long-range order in the system is expressed by Fourier transform of the structural units – ORs and ARs [terms $F(\boldsymbol{\chi})^{\mathrm{AR}}$ and $F[\boldsymbol{\chi})^{\mathrm{OR}}$ in (25)], whereas atomic decoration of the units is revealed in the phase factors [exponentials in (25)]. In other words, the full structural information of the system is expressed by the formula (25). The correctness of the formula obtained was confirmed against numerical 'reference' data for structural units decorated in vertices.

The structure-factor formula is ready to be applied to the refinement procedure of the real structure of i-QCs. First, the so-called simple decoration model (Henley & Elser, 1986) will be considered and then structure refinement of systems like i-Cd–Yb (Takakura *et al.*, 2007) will be attempted.

APPENDIX *A*
Orientations of structural units

In this part we show that only ten orientations of ORs and ARs in three-dimensional reciprocal space are inequivalent. This observation is also true for three-dimensional physical space. Let us perform the symmetry consideration in reciprocal space, where the basis vectors $\mathbf{B}^*$ span a Platonian icosahedron (Fig. 3). Each OR is spanned by vectors $\mathbf{d}_1^*, \mathbf{d}_2^*, \mathbf{d}_6^*$ and each AR by vectors $\mathbf{d}_1^*, \mathbf{d}_3^*, \mathbf{d}_6^*$ [the reciprocal basis is defined by relation (3)]. The definition of ORs and ARs in physical space is analogous.

Although there are only two independent units, they can both occur in different orientations induced by icosahedral symmetry. In order to designate the number of inequivalent orientations and positions of rhombohedra let us have a closer look at the shape of an icosahedron. ORs can be labelled by the faces of an icosahedron (vectors spanning rhombohedra are pointing towards vertices of the icosahedron) and grouped according to the fivefold symmetry axis. In Fig. 12 the projections of ORs onto faces of an icosahedron are presented.

An icosahedron has 20 faces; therefore 20 independent orientations of ORs are technically possible. However, the inversion symmetry limits the number of independent orientations to ten. According to Fig. 12, ORs belonging to a group of faces marked with crosses are equivalent to the ones marked with stripes. The same applies to faces marked with circles and a grid.

The orientations of ARs can also be presented as projections on the facets of an icosahedron. Six possible orientations

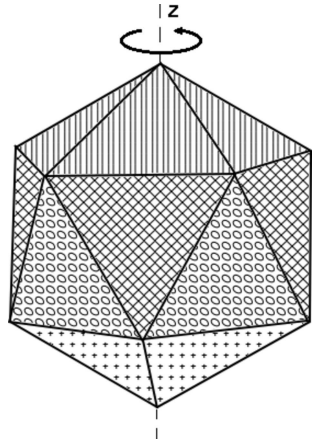

Figure 12
Orientations of ORs adjacent to faces of a Platonian icosahedron. Four groups of ORs symmetrically equivalent with respect to the fivefold rotation axis are distinguished. Each face being representative of the group is marked with a different pattern. Inversion neglected.

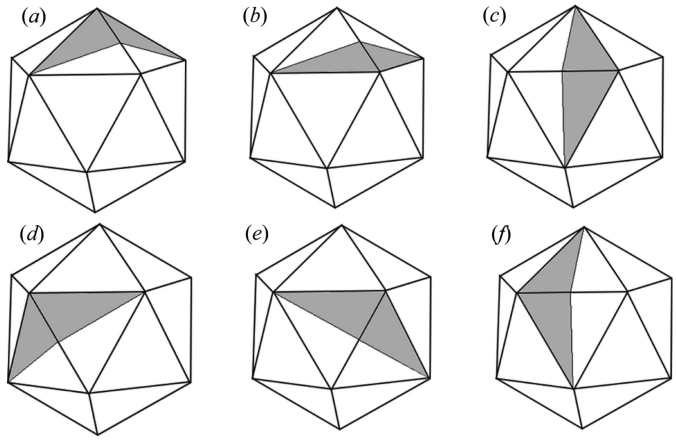

Figure 13
Possible orientations of ARs represented as corresponding faces of an icosahedron. Inversion neglected.

Table 4
Exact results of analytical integration of Fourier transforms in formula (23).

Notation explained in the text of the main article.

Case	q_j values ($j \in \{1, 2, 3\}$)	Fourier transform
1	$q_1, q_2, q_3 \neq 0$	$F(\mathbf{k}) = V\dfrac{i}{q_1 q_2 q_3}[\exp(iq_1X) - \exp(iq_1X_O)][\exp(iq_2Y) - \exp(iq_2Y_O)][\exp(iq_3Z) - \exp(iq_3Z_O)]$
2	$q_1 = 0$	$F(\mathbf{k}) = -V\dfrac{X - X_O}{q_2 q_3}[\exp(iq_2Y) - \exp(iq_2Y_O)][\exp(iq_3Z) - \exp(iq_3Z_O)]$
3	$q_2 = 0$	$F(\mathbf{k}) = -V\dfrac{Y - Y_O}{q_1 q_3}[\exp(iq_1X) - \exp(iq_1X_O)][\exp(iq_3Z) - \exp(iq_3Z_O)]$
4	$q_3 = 0$	$F(\mathbf{k}) = -V\dfrac{Z - Z_O}{q_1 q_2}[\exp(iq_1X) - \exp(iq_1X_O)][\exp(iq_2Y) - \exp(iq_2Y_O)]$
5	$q_1, q_2 = 0$	$F(\mathbf{k}) = -iV\dfrac{(X - X_O)(Y - Y_O)}{q_3}[\exp(iq_3Z) - \exp(iq_3Z_O)]$
6	$q_1, q_3 = 0$	$F(\mathbf{k}) = -iV\dfrac{(X - X_O)(Z - Z_O)}{q_2}[\exp(iq_2Y) - \exp(iq_2Y_O)]$
7	$q_2, q_3 = 0$	$F(\mathbf{k}) = -iV\dfrac{(Y - Y_O)(Z - Z_O)}{q_1}[\exp(iq_1X) - \exp(iq_1X_O)]$
8	$q_1, q_2, q_3 = 0$	$F(\mathbf{k}) = V(Z - Z_O)(Y - Y_O)(X - X_O)$

invariant to the inversion centre are presented in Fig. 13. Each AR occurs in five orientations according to fivefold symmetry. That gives 30 orientations. However, still some repeating orientations occur. This is because the two adjacent faces representing given orientations of rhombohedra are included. It is easy to notice that group (*b*) of rhombohedra can be retrieved from group (*d*) by rotation by an angle of $2\pi/5$ along one of the fivefold axes (see Fig. 14). They share the same edge *AB* which means that rhombohedra belonging to these groups are spanned by the same two basis vectors. Moreover, vertices *C* and *C*′ are symmetric with respect to the inversion centre of an icosahedron, which implies that both ARs (*CBA* and *ABC*′) are symmetrically equivalent. The same applies to group (*e*), whereas groups (*a*), (*c*) and (*f*) represent another orientation of ARs. Summarizing, only ten inequivalent orientations of ARs occur under the icosahedral symmetry.

APPENDIX *B*
Fourier transforms of subdomains – exact results

Fourier transforms of subdomains in perpendicular space can be calculated with formula (23). The results of integration strongly depend on the values of q_j [$q_j = \mathbf{k}^{\perp}\mathbf{e}_j$, $j \in \{1, 2, 3\}$, where vectors $\mathbf{e}_j$ span rhombohedral subdomains (see Fig. 10*a*)]. Detailed case studies of integral (23) were performed and the exact analytical results are shown in Table 4.

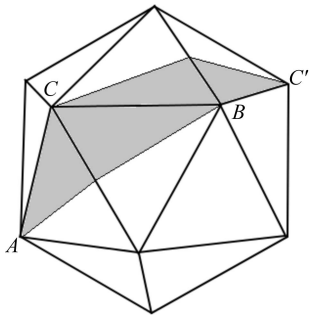

Figure 14
Representations of two symmetrically inequivalent orientations (*ABC*′ and *CBA*) of ARs.

Acknowledgements

The authors acknowledge financial support from the Polish National Science Centre (NCN) under grant No. DEC-2013/11/B/ST3/03787. RS has been partly supported by the EU Human Capital Operation Program, Polish Project No. POKL.04.0101-00-434/08-00. We are very grateful to Pawel Kuczera for final editing of the manuscript.

References

Baake, M. & Grimm, U. (2013). *Aperiodic Order*, Vol. 1, *A Mathematical Invitation*. Cambridge University Press.
Bruijn, N. G. de (1981). *Ned. Akad. Wet. Proc. Ser. A*, **84**, 38–66.
Henley, C. L. & Elser, V. (1986). *Philos. Mag. B*, **53**, L59.
Kozakowski, B. (2007). PhD thesis, AGH University of Science and Technology, Krakow, Poland.
Kozakowski, B. & Wolny, J. (2010). *Acta Cryst.* A**66**, 489–498.
Kramer, P. & Neri, R. (1984). *Acta Cryst.* A**40**, 580–587.
Kuczera, P., Wolny, J., Fleischer, F. & Steurer, W. (2011). *Philos. Mag.* **91**, 2500–2509.
Kuczera, P., Wolny, J. & Steurer, W. (2012). *Acta Cryst.* B**68**, 578–589.
Kuczera, P., Wolny, J. & Steurer, W. (2014). *Acta Cryst.* B**70**, 306–314.
Levine, D. & Steinhardt, P. J. (1984). *Phys. Rev. Lett.* **53**, 2477–2480.
Levine, D. & Steinhardt, P. J. (1986). *Phys. Rev. B*, **34**, 596–616.
Oosterom, A. van & Strackee, J. (1983). *IEEE Trans. Biomed. Eng.* **BME-30**, 125–126.
Shechtman, D., Blech, I., Gratias, D. & Cahn, J. W. (1984). *Phys. Rev. Lett.* **53**, 1951–1953.
Steinhardt, P. J. & Ostlund, S. (1987). *The Physics of Quasicrystals*. Singapore: World Scientific.
Steurer, W. & Deloudi, S. (2009). *Crystallography of Quasicrystals*. Berlin, Heidelberg: Springer.

Strzałka, R. & Wolny, J. (2014). *Acta Phys. Pol. A*, **126**, 585–587.
Strzalka, R., Wolny, J. & Kuczera, P. (2013). *Aperiodic Crystals*, edited by S. Schmid, R. L. Withers & R. Lifshitz, pp. 203–210. Dordrecht, Heidelberg: Springer Science+Business Media.
Takakura, H. (2008). *Philos. Mag.* **88**, 1905–1912.
Takakura, H., Gomez, C. P., Yamamoto, A., de Boissieu, M. & Tsai, A. P. (2007). *Nat. Mater.* **6**, 58–63.
Wolff, P. M. de, Janssen, T. & Janner, A. (1981). *Acta Cryst.* A**37**, 625–636.
Wolny, J. (1998*a*). *Acta Cryst.* A**54**, 1014–1018.
Wolny, J. (1998*b*). *Philos. Mag. A*, **77**, 395–412.
Wolny, J., Kozakowski, B., Kuczera, P. & Strzalka, R. (2013). *Aperiodic Crystals*, edited by S. Schmid, R. L. Withers & R. Lifshitz, pp. 211–218. Dordrecht, Heidelberg: Springer Science+Business Media.
Wolny, J., Kozakowski, B., Kuczera, P., Strzalka, R. & Wnek, A. (2011). *Isr. J. Chem.* **51**, 1275–1291.
Yamamoto, A. (1996). *Acta Cryst.* A**52**, 509–560.